Lab on a Chip

PAPER

View Article Online
View Journal

Cite this: DOI: 10.1039/d0lc01013h

A 3-dimensional microfluidic platform for modeling human extravillous trophoblast invasion and toxicological screening†

Yong Pu,[a] Jeremy Gingrich[b] and Almudena Veiga-Lopez *[a]

Received 7th October 2020,
Accepted 2nd November 2020

DOI: 10.1039/d0lc01013h

rsc.li/loc

Placental trophoblast cells invasion into the maternal uterus is an essential and complex event in the formation of the maternal–fetal interface. Commonly used two-dimensional (2D) cell invasion tools do not accurately represent the *in vivo* cell invasion microenvironment. Three-dimensional (3D) silicone polymer polydimethylsiloxane (PDMS) microfluidic platforms are an emerging technology in developing organ-on-a-chip models. Here, we present a placenta-on-a-chip platform that enables the evaluation of trophoblast invasion with intraluminal flow within an engineered PDMS 3D microfluidic chip. This platform reproduces key elements of the placental microenvironment, including endothelial and trophoblast cells, layered with an extracellular matrix, and incorporates dynamic medium flow while allowing for real-time monitoring, imaging, evaluation of trophoblast cell invasion, and heterocellular cell-to-cell interactions. Coupled with fluorescent cell tagging and flow cytometry, this platform also allows collection of the invasive cells. This will help our understanding of pathways that regulate trophoblast cell invasion and may prove important for toxicological screening of exposures that interfere with invasiveness in a complex organ such as the placenta.

Introduction

The placenta is a transient organ that originates from the blastocyst's trophectoderm layer. To facilitate uterine implantation, placental cytotrophoblast cells differentiate into invasive cells known as extravillous trophoblast (EVTs). EVTs proliferate and migrate towards the maternal endometrium and invade into the decidualized uterus to develop a maternal–fetal blood exchange system.[1] While this process starts at day 35 of pregnancy in humans,[2] complete maternal–fetal exchange is not finalized until the end of the first trimester.[2] Proper EVT invasion is critical for conceptus attachment and placenta development.[1] Defects of EVT invasiveness can result in deficient spiral artery remodeling, which is associated with abnormal placentation and pregnancy outcomes, such as the development of pre-eclampsia,[3] fetal growth restriction,[4] and early pregnancy loss.[5] *In vivo*, EVTs invade into the neighboring decidualized uterus, composed of endometrial stromal cells, uterine glands, blood vessels, and immune cells. EVT invasion involves cell-to-cell interactions with stromal cells, macrophages and decidual natural killer cells; a process regulated by cytokines, hormones, and growth factors.[6–10]

Given the complexity of studying human placental trophoblast invasion during early pregnancy *in vivo*, understanding trophoblast invasion has been largely based on *in vitro* models. Developed in 1987,[11] the transwell invasion model continues to be among the most widely used trophoblast cell invasion models. The transwell model uses Matrigel, a gelatinous protein mixture, to mimic the extracellular matrix, and assesses cell invasiveness by quantifying cells that cross the Matrigel layer, often towards a chemoattractant. Although the transwell system partly recreates the extracellular matrix environment, other factors that play a key role in the *in vivo* environment are not well captured, including 1) interactions among different cell types, 2) shear stress, and 3) continuous flow of nutrient supply.[12] Recently, three-dimensional (3D) invasion models have been developed, such as the 3D cell tracking assay model, vertical gel invasion assay model, spheroid/monodispersed cell invasion assay model, spheroid confrontation assay model, and spheroid gel invasion assay model.[13–15] However, one of the major limitations of these 3D models is the lack of a continuous flow of nutrient supply, a caveat that can be addressed by the use of microfluidics. This emerging technology has allowed the development of organ-on-a-chip models in numerous organ systems, including lung, kidney, brain and placenta, among others.[16,17] Some of these models

[a] Department of Pathology, University of Illinois at Chicago, 909 S. Wolcott Ave, Rm 6093, Chicago, IL, 60612, USA. E-mail: veiga@uic.edu
[b] Department of Pharmacology and Toxicology, Michigan State University, USA

† Electronic supplementary information (ESI) available. See DOI: 10.1039/d0lc01013h

have been proven to be a useful tool in exploring the effects of toxicological exposures. For instance, a microfluidic small airway-on-a-chip reflects the response of the epithelium to smoke exposure.[18]

Several placenta-on-a-chip 3D microfluidic models have been developed to understand placental syncytialization using a co-culture of human endothelial (HUVEC) and placental choriocarcinoma cells (BeWo).[19,20] More recently, other 3D placenta-on-a-chip models have been developed to evaluate drug transport across the placenta barrier by co-culturing human endothelial cells and BeWo cells.[21,22] Given that cell invasiveness is necessary for proper placental development[1] and that defects in trophoblast invasiveness have been associated with abnormal placentation and pregnancy outcomes,[3–5] our goal was to develop a microfluidic 3D platform to evaluate placenta cells invasiveness. A 3D microfluidic model has been previously reported to test human placental trophoblast cell invasion.[23] This model embedded primary human trophoblast cells in Matrigel and recreated a microenvironment that allowed for a chemical gradient across the hydrogel channel, and included immune cells to modulate trophoblast migration.[23] This 3D system could be further improved with the inclusion of a heterogenous cellular microenvironment to understand trophoblast–endothelial cell interactions, and the establishment of an endothelial barrier to allow for an active diffusion gradient, which were goals of this study.

In the current study, we have used a commercially-available 3D microfluidic chip, fluorescent protein-tagged human first trimester placenta cells (HTR8/SVneo) and human umbilical vein endothelial cells (HUVECs) to develop a 3D microfluidic placenta-on-a-chip model that mimics the *in vivo* trophoblast microenvironment relative to the trophoblast–endothelial cell interaction. This 3D microfluidic chip incorporates many of the advantages that 3D models offer, like continuous medium flow, shear stress, presence of ECM layer, and real-time cellular monitoring. This model, additionally, incorporates improvements to previously reported invasion models through inclusion of trophoblast and endothelial cells, an endothelial barrier, and fluorescent-tagged cells to allow for real-time monitoring and cell harvest through flow cytometry. These improvements allow for the application of this model system for toxicological screenings.

Methods

Cell culture

Trophoblast and endothelial cells were used to develop an *in vitro* 3D placental microfluidic culture system that would recapitulate the human placental microenvironment. The chorionic villi-derived first-trimester human placenta HTR8/SVneo trophoblast cell line (CRL-3271, ATCC, Manassas, VA, USA), commonly used as a trophoblast cell model.[14,24,25] While this cell line has been reported to include a heterogeneous cell population,[26] it continues to be used as the primary cell model for trophoblast cell invasion studies.[14,27,28] Cells were proliferated by seeding them into 100 mm plates at 500 000 cells per dish and cultured in growth medium (DMEM/F12 supplemented with 1% penicillin–streptomycin, 2 mM L-glutamine, 10% FBS, and 10 mM HEPES) at 37 °C, 5% CO_2. Human umbilical vein endothelial cells (HUVECs, CC-2935, Lonza, Minneapolis, MN, USA) were used as the endothelial cell layer and were grown in complete medium (basal medium (CC-3156, Lonza, Minneapolis, MN, USA) supplemented with EGM-2 Plus medium (CC-4176, Lonza, Minneapolis, MN, USA)). All reagents were purchased from Thermo Fisher unless otherwise stated.

3D microfluidic chip

The 3D microfluidic chip (Fig. 1A, cat#: 102008, SynVivo, Huntsville, AL, USA) is composed of silicone polymer polydimethylsiloxane (PDMS). It includes a central circular compartment (connected to two inlet ports and two outlet ports; Fig. 1B) with two outer channels (200 μm in width, with an inlet and an outlet port; Fig. 1B) surrounding it. The barrier (50 μm in width) between the central compartment and both outer channels is composed of pillars (pillar spacing: 3 μm; Fig. 1C). Before use, the microfluidic chip needs to be primed with DPBS in vacuum and then coated with the extracellular matrix (ECM) which allows for attachment and invasion of trophoblast cells (see next sections for details).

Microfluidic 3D chip priming, coating, and cell seeding

Before use, the 3D microfluidic chip was primed with DPBS to devoid the chip of air. The chip was then submerged in DPBS in a petri dish and placed into a vacuum desiccator pump (model DOA-P104-AA, GAST, Benton Harbor, MI, USA) for 1 h. The central compartment and two outer channels of the microfluidic chip were coated with an ECM using a 1 ml syringe. Thereafter, all inlet and outlet ports were clamped and allowed to settle overnight at 4 °C. ECM pre-coated chips were then warmed up for 30 min at room temperature, and the central compartment and outer channels manually seeded with freshly harvested HUVEC and HTR8/SVneo cells, respectively. Cell confluency was assessed after 24 h incubation (37 °C, 5% CO_2, 100% humidity).

Optimization of the extracellular matrix

To test the best suitable ECM in our model, ECM optimization for trophoblast (HTR8/SVneo) and endothelial cells (HUVECs) was conducted by testing three matrices: 1) gelatin (cat#: G1890, Sigma, St. Louis, MO, USA), 2) Matrigel (cat#: 354234, Corning, Tewksbury, MA, USA) and 3) fibronectin (cat#: 33016-015, Gibco, Van Allen Way Carlsbad, CA, USA). For all three matrices, both HTR8/SVneo and HUVECs were seeded in pre-coated 30 mm petri dishes with gelatin (0.2% w/v), Matrigel (1 mg ml^{-1}) or fibronectin (200 μg ml^{-1}) for 1 h at 37 °C. After 2, 3, or 4 h of culture, cells were fixed with 10% neutral-buffered

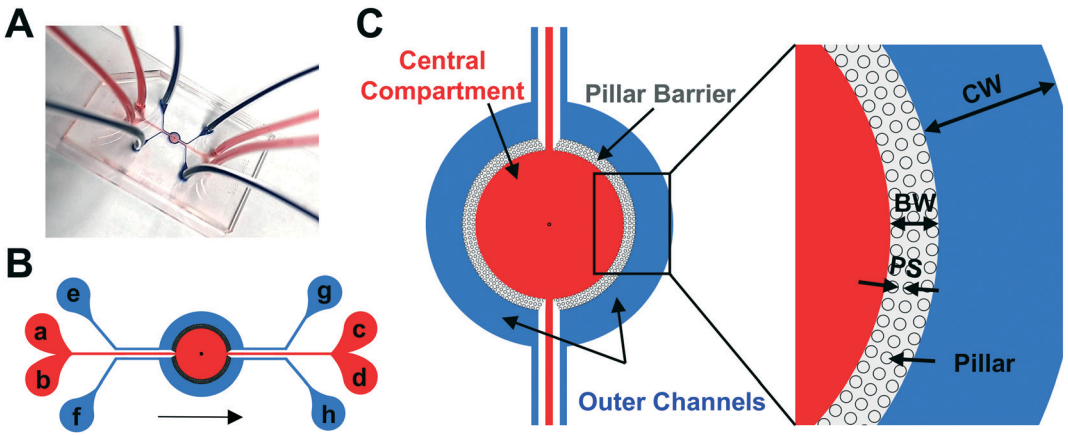

Fig. 1 A. Silicone polymer polydimethylsiloxane (PDMS) 3D microfluidic chip. B. 3D microfluidic chip scheme depicting the following components: 1) a central compartment (red) with a central feeder line supplied by two inlet ports (a and b) connected to two outlet ports (c and d); 2) two outer channels (blue) with two outer feeder lines supplied by two inlet ports (e and f) connected to two outlet ports (g and h), and a 3) pillar barrier in between. Arrow corresponds to the directionality of medium flow. C. Close up scheme of the center of the 3D microfluidic chip with the central compartment (red), outer channels (blue, width (CW): 200 μm), and pillar barrier (width (BW): 50 μm), filled with pillars (pillar spacing (PS): 3 μm).

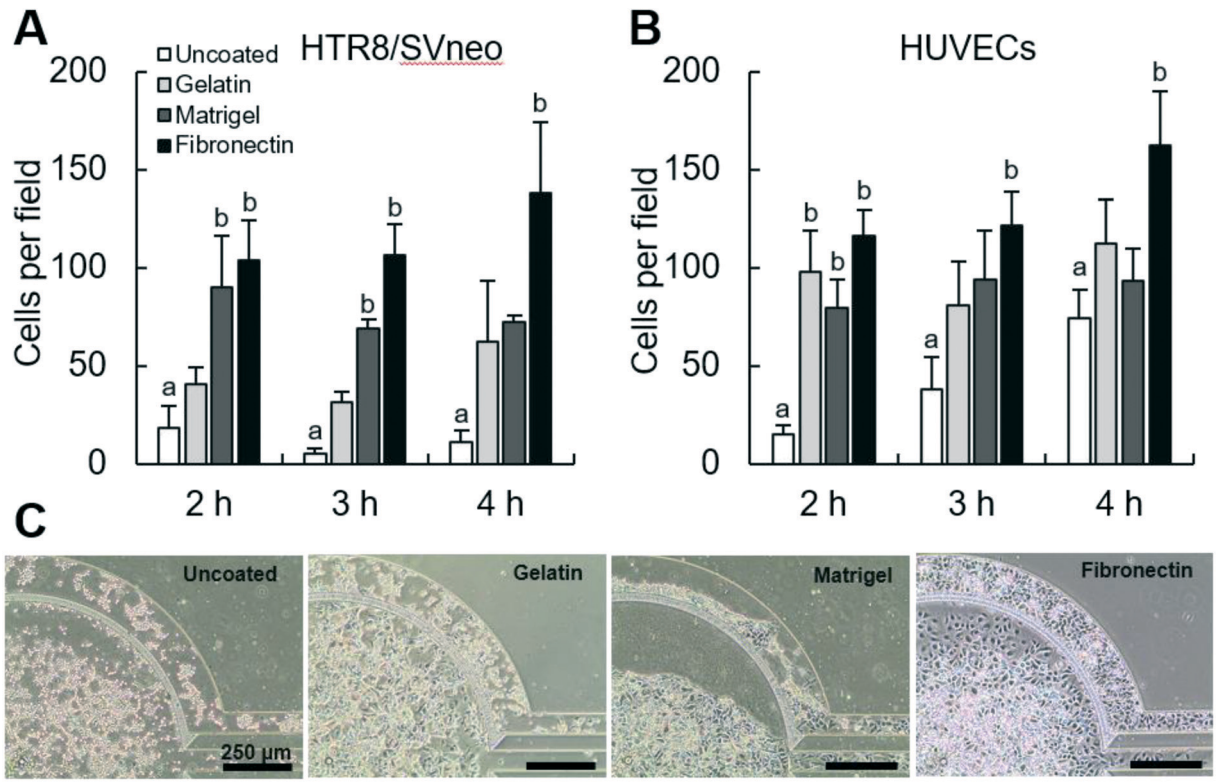

Fig. 2 Cell adhesion in ECM coated dishes and 3D-microfluidic chips. Top panels. Cell adhesion for HTR8/SVneo trophoblast cells (A) and human umbilical vein endothelial cells (HUVECs) (B) were compared to uncoated dishes after seeding into the gelatin, Matrigel and fibronectin coated 60 mm dishes for 2, 3, and 4 h (A and B) after seeding. Different letters denote differences among groups (a ≠ b denote $P < 0.05$). Bottom panel (C). Cell adhesion for HTR8/SVneo trophoblast cells and human umbilical vein endothelial cells (HUVECs) was compared to uncoated 3D microfluidic chip after seeding into the gelatin, Matrigel and fibronectin coated chips 4 h after seeding.

formalin (cat#: HT501128; Sigma, St. Louis, MO, USA), and the unattached cells gently washed out with DPBS. The attached cells were stained with DAPI and imaged (TE2000-U, Nikon, Tokyo, Japan). The number of attached cells was assessed by counting DAPI-positive nuclei and quantified with Image J (version 1.48). To further validate these results in the 3D microfluidic chip, the chips were pre-coated with gelatin (0.2% w/v), Matrigel (1 mg ml^{-1}), or fibronectin (200 μg ml^{-1}) overnight at 4 °C and HTR8/SVneo and HUVECs were seeded into the outer channels and central compartment of the 3D microfluidic chip, respectively. After 4 h of culture, cells in 3D microfluidic chips were fixed to offer a visual comparison of cell attachment between groups.

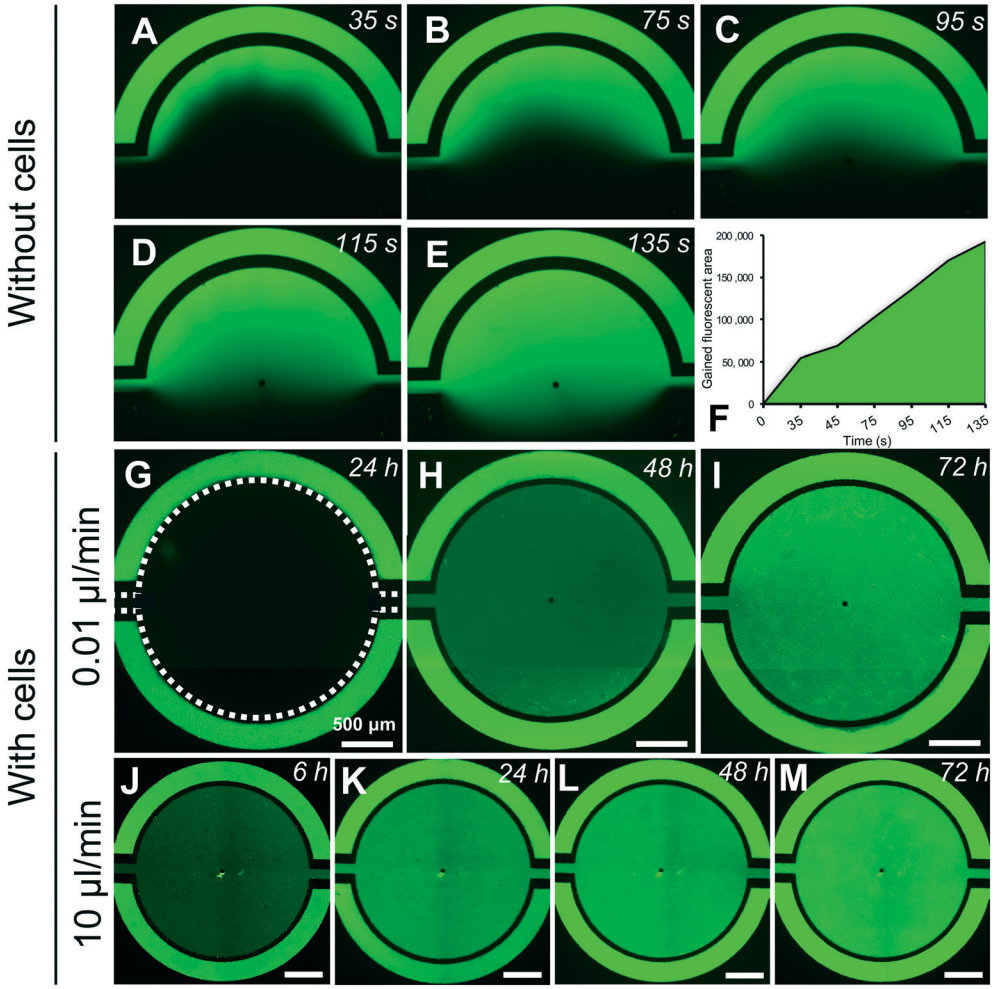

Fig. 3 Microfluidic barrier permeability to FITC-dextran (25 µg ml^{-1}) without (A–E) and with cells (G–M) seeded in the 3D microfluidic chip. 3D microfluidic chip permeability after 35, 75, 95, 115, and 135 seconds (s) (A–E), and 24 h (G), 48 h (H) and 72 h (I) of constant dextran flow without cells seeded (A–E) and with cells seeded (G–M) in both, the central compartment (HUVECs) and the outer channels (HTR8/SVneo). The permeability, measured as fluorescence area in the central compartment, was quantified after constant dextran flow for 35, 75, 95, 115 and 135 s (F). 3D microfluidic chip permeability after 6 h (J), 24 h (G and K), 48 h (H and L) and 72 h (I and M) of constant dextran flow with cells seeded in the chip. Dotted line in panel G represents the outline of the central compartment. Note that cells can be observed within the outline of the central compartment (H–M), while cells are not visible in the outer channels due to the high FITC-dextran concentration.

Optimization of the cell seeding density and flow speed

To optimize cell density and medium flow speed within each compartment of the microfluidic chip, three cells seeding densities (10, 20, or 30 million cells per ml) and three flow speeds (0.01, 0.05 or 0.1 µl min^{-1}) were tested. After 24 h, media flow was started in all three compartments using a syringe pump (cat#: 70-3007, Harvard Apparatus; Holliston, MA, USA). After 24 h, cell density was assessed in all microfluidic chip compartments. Cell seeding density and flow speed resulting in the highest cell attachment was chosen as the optimal culture conditions. All treatments were run in triplicate. The circularity of the microfluidic chip resulted in shear stress to occur within the device. For each flow speed, shear stress within the microfluidic chip was calculated as $\tau = \mu \times \gamma$; where τ is the calculated shear stress, μ is the dynamic viscosity and γ is the shear rate for a channel height and width of 100 and 200 µm, respectively. Dynamic viscosity for DMEM supplemented with 10% FBS was assumed at 0.00094 kg m^{-1} s^{-1}.[29]

Cell invasion in the 3D microfluidic chip

To test cell invasion in the 3D microfluidic chip, trophoblast cells (mCherry tagged, see section below) were pre-treated for 48 h with vehicle (DPBS, 0.1% v/v), or folic acid (100 ng ml^{-1}, 0.1% v/v. >97%; Sigma, St. Louis, MO, USA), a chemoattractant which can stimulate HTR8/SVneo cells invasion.[30] Cells were also co-treated with folic acid plus tunicamycin (50 ng ml^{-1}, 0.05% v/v.; Sigma, St. Louis, MO, USA), which can inhibit placenta cells invasion.[31] Thereafter, ECM pre-coated 3D microfluidic chips were warmed up to room temperature and seeded with HUVECs in the central compartment and mCherry tagged HTR8/SVneo cells in both

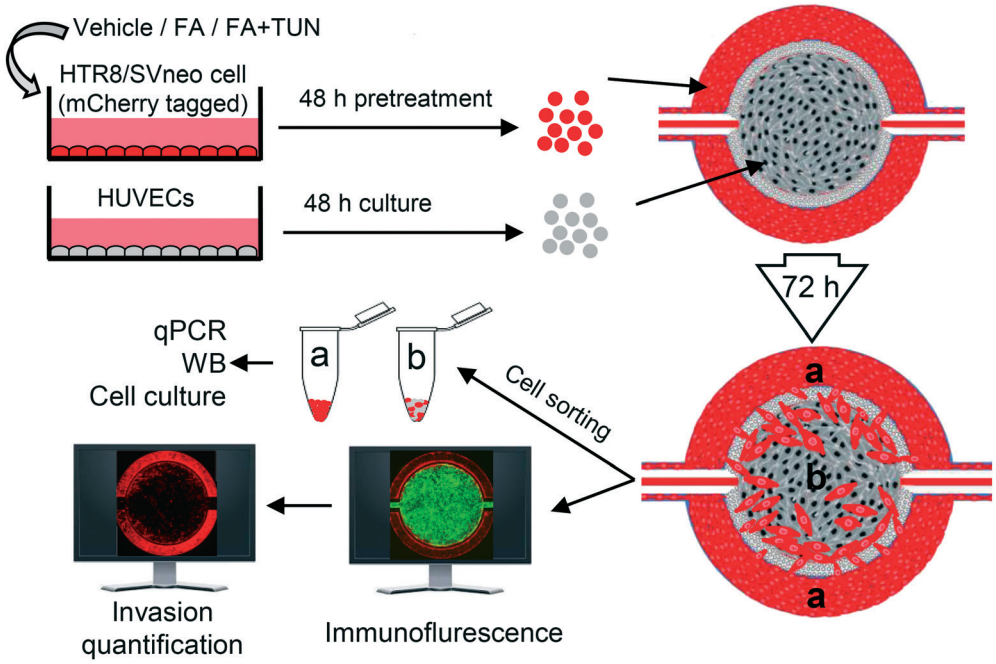

Fig. 4 Scheme of the experimental design used in the study for cell invasion in the 3D microfluidic chip. HTR8/SVneo cells were pre-treated with folic acid (FA), or FA + TUN (tunicamycin) for 48 h and seeded into the outer channels. HUVECs were cultured for 48 h and then seeded into the central compartment. After 72 h of culture (culture conditions: fibronectin, 30 million cells per ml, and 0.01 μl min^{-1} flow speed), invading mCherry tagged HTR8/SVneo cells can be imaged under the fluorescence microscope, fixed for immunostaining, or trypsin harvested for cell sorting and further analysis, such as further culture, real-time quantitative PCR (qPCR) or western blot (WB).

outer channels. The central compartment was flushed with HUVEC medium supplemented with 10% FBS and folic acid or folic acid plus tunicamycin. The outer channels were flushed with HTR8/SVneo cell medium with low serum (1%) and supplemented with folic acid or folic acid plus tunicamycin. The number of HTR8/SVneo cells that invaded into the central compartment were quantified at 24, 48, and 72 h (TE2000-U, Nikon, Tokyo, Japan). To test whether the presence of the endothelial cells will affect HTR8/SVneo cell invasiveness, we exposed HTR8/SVneo cells in the 3D microfluidic chip to folic acid, tunicamycin or the combination of folic acid and tunicamycin (same doses as above) in the absence of HUVEC cells in the central compartment. HTR8/SVneo cells that invaded into the central compartment were quantified after 72 h. All treatments were run in triplicate.

Cell viability assay

Cell viability was determined using an MTT assay as previously described.[32] In brief, HTR8/SVneo cells were seeded into 96-well plates (1000 cells per well) and cultured overnight in growth medium. After attachment, cells were treated with folic acid (0, 10, 100, 200, 500 ng ml^{-1}) or tunicamycin (0, 10, 50, 100, 200, 500 ng ml^{-1}) in growth medium for 5 days. Folic acid was dissolved in 1 M NaOH. After a 4 h incubation with MTT working solution, the cell viability was determined by absorbance quantification at 570 nm using a microplate reader (SpectraMax M5e, Molecular Devices LLC, Sunnyvale, CA, USA). All treatments were run in triplicate.

Permeability assay

Permeability between the central compartment and outer channels was tested after priming and before and after ECM coating and cell seeding. A FITC-dextran (4 kDa, cat#: 46944, Sigma, St. Louis, MO, USA) working solution (25 μg ml^{-1}, in DMEM/F12) was pumped into the outer channels at two different speeds (0.01 or 10 μl min^{-1}). Transfer of FITC-dextran between the compartment and channels was recorded at 35, 75, 95, 115, and 135 s in a chip devoided of cells, and 6, 24, 48, 72 h in a cell seeded chip by using a fluorescence microscope (TE2000-U, Nikon, Tokyo, Japan).

Fluorescence tagged HTR8/SVneo and HUVEC cells

Stable expression of mCherry protein in HTR8/SVneo cells and GFP protein in HUVECs was induced *via* lentiviral transduction. The lentiviral particles were generated in HEK293T (cat#: CRL-3216, ATCC, Gaithersburg, MD, USA) cells with a second-generation packaging system and pLVX-mCherry-C1 vector (Takara Bio, California, USA). In brief, HEK293T cells were seeded into a 100 mm cell culture dish, and the plasmids of psPAX2 (3 μg), PMD2G (3 μg) and pLVX-mCherry or -eGFP (2 μg) were transfected into HEK293T cells using Fugene 6 (cat#: E2692, Promega, Madison, WI, USA) in a 500 μl transduction volume at 60% confluency. After overnight incubation, the transfection medium was replaced

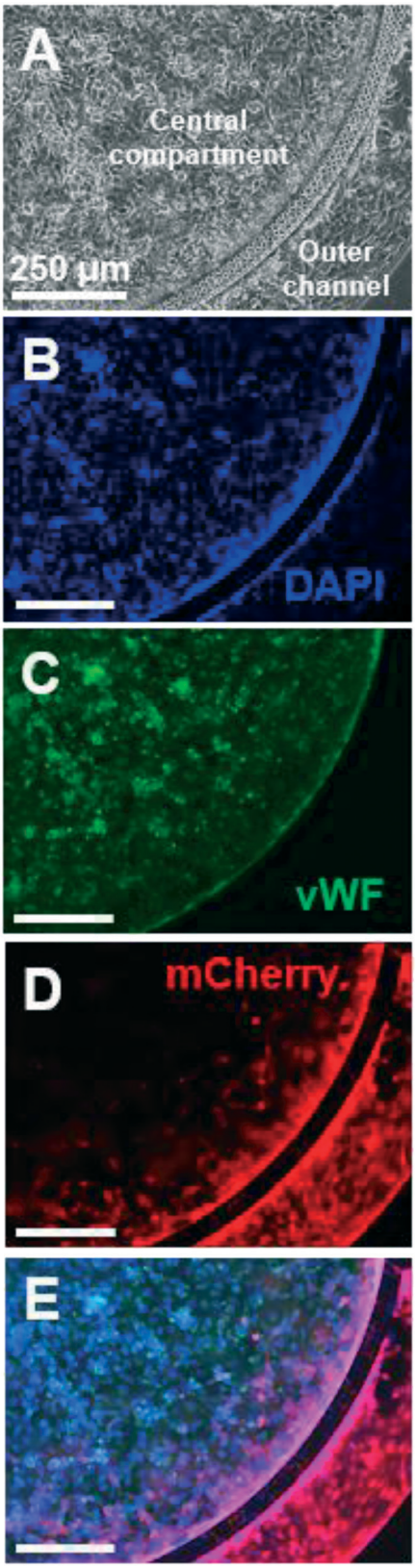

Fig. 5 3D microfluidic chip immunofluorescence of HTR8/SVneo (outer channels) and HUVECs (central compartment) after 72 h of culture (fibronectin, 30 million cells per ml, and 0.01 µl min^{-1} flow speed). Bright field (A), DAPI nuclear stain (B), HUVECs immunostained for von Willebrand factor (vWF, C), mCherry-tagged HTR8/SVneo cells (D) and merged images (E).

with fresh growth medium (DMEM/F12 supplemented with 10% FBS and 10 mM HEPES) and cells cultured for 72 h. Thereafter, the supernatant was collected, and viral particles concentrated with Lenti-X concentrator (cat#: 631231, Takara, Mountain View, CA, USA). HTR8/SVneo cells and HUVEC cells were then transduced with the mCherry- and eGFP-viral particles, respectively and placed in growth medium supplemented with puromycin (1 µg ml^{-1}, cat#: P9620, Sigma, St. Louis, MO, USA). After 7 days of selection, cells with stable expression of mCherry and eGFP were harvested and frozen until further use.

Immunofluorescence

All cells were fixed with formalin and stained with either the endothelial cell marker von Willebrand factor (vWF, cat#: ab6994, Abcam, UK) for HUVECs identification or the transmigration marker intercellular adhesion molecule 1 (ICAM-1, cat#: ab109361, Abcam, Cambridge, MA, USA). As previously described,[32] cells were incubated with primary antibodies vWF (1 : 400 dilution) and ICAM-1 (1 : 100 dilution) overnight at 4 °C. After DPBS washes, cells were incubated with an Alexa Fluor 488-conjugated secondary antibody (cat#: 111-545-003, Jackson Immuno Research Labs, West Grove, PA, USA) or Alexa Fluor 647-conjugated secondary antibody (cat#: A21244, Invitrogen, Carlsbad, CA, USA) for 1 h at 37 °C in the dark. Cells were then counterstained with DAPI nuclear stain for 5 min and imaged with a fluorescence microscope (TE2000-U, Nikon, Tokyo, Japan).

Matrix degradation assay

To demonstrate HTR8/SVneo cells invasiveness we performed a cell degradation matrix assay as previously described.[33] In brief, 96-well plates were coated with Oregon Green® 488-conjugated gelatin (60 µl per well, cat#: G13186, Thermo Fisher, Waltham, MA, USA; 1 mg ml^{-1}) for 4 h at room temperature. The wells were then seeded with HTR8/SVneo-mCherry cell (1000 cells per well) and cultured for 24 h. The wells were imaged with a fluorescence microscope (TE2000-U, Nikon, Tokyo, Japan). The proteolytic degradation of the matrix, a critical step in cellular invasion, was visualized by the reduction of Oregon Green® 488 signal.

Real-time quantitative PCR (RT-qPCR)

Total RNA extraction and reverse transcription into cDNA and relative mRNA expression of the genes encoding matrix metallopeptidase 2 (MMP2) were performed as previously described.[34] Primer sequences are provided in Table S1.† All RT-qPCR runs were done in triplicate. mRNA levels encoding the indicated genes were normalized against GAPDH and presented as a relative fold change to that of the control. Melt curve analyses were performed for all genes, and both the specificity as well as integrity of the PCR products were confirmed by the presence of a single peak and single-PCR product band by gel electrophoresis.

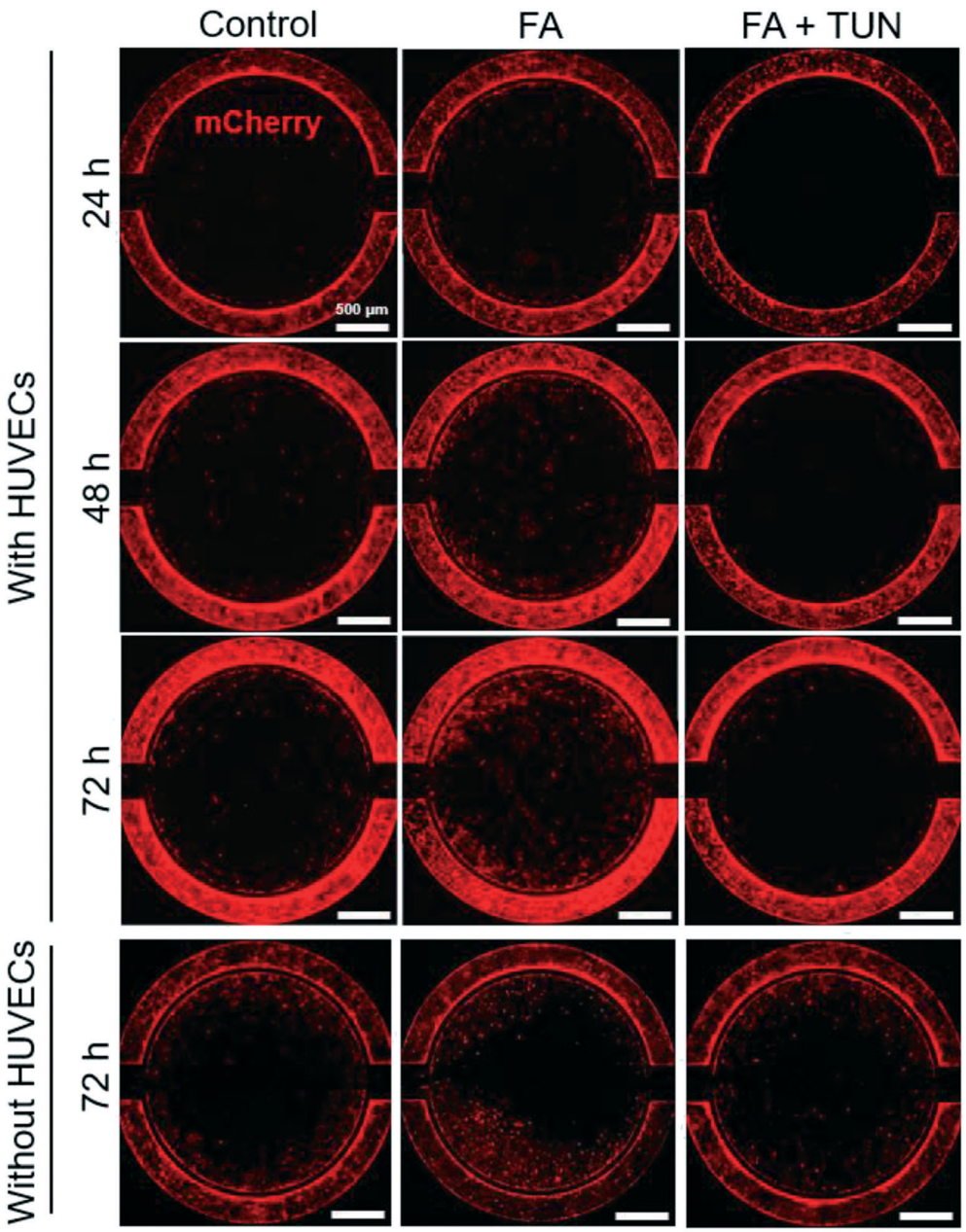

Fig. 6 Cell invasion in the 3D microfluidic chip. The effect of control (vehicle, DPBS), folic acid (FA, 100 ng ml^{-1}) and FA (100 ng ml^{-1}) plus tunicamycin (TUN, 50 ng ml^{-1}) on mCherry-tagged HTR8/SVneo cells invasion after 24, 48 and 72 h exposure in the 3D microfluidic chip with (top 3 panels) or without HUVECs (bottom panel) seeded in the central compartment (culture conditions: fibronectin, 30 million cells per ml, and 0.01 μl min^{-1} flow speed).

Flow cytometry

After three days of invasion in the 3D microfluidic chip, the cells in the central compartment were trypsin harvested, spun down and resuspended in DPBS containing 3% bovine serum albumin (Sigma-Aldrich, St. Louis, MO, USA) at a concentration of 2×10^5 cells per ml. The wild type and mCherry tagged HTR8/SVneo cells were used as negative and positive controls, respectively. Samples (single cell suspensions) were processed using a fluorescence-activated cell sorting (FACS) flow cytometer (BD Biosciences, San Jose, CA, USA) and analyzed with BD FACS software (version of 1.00.650). All treatments were run in triplicate.

Transwell invasion assay

HTR8/SVneo cells were pretreated with folic acid (100 ng ml^{-1}, 0.1% v/v) or folic acid plus tunicamycin (50 ng ml^{-1}, 0.1% v/v) for 48 h. Matrigel pre-coated transwell cell culture inserts (24-wells, 8 μm pore size, Corning, Tewksbury, MA, USA) were placed in a 24-well plate and pre-warmed 20 min at room temperature and then rehydrated for 2 h. Cells were

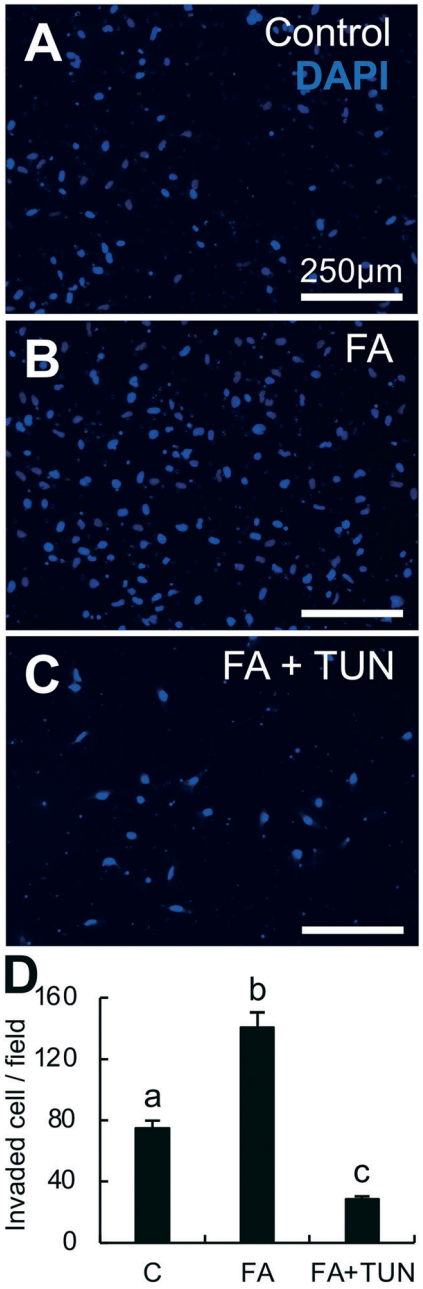

Fig. 7 HTR8/SVneo cell invasion in a transwell after 18 h exposure to the control (vehicle, DPBS) (A), folic acid (FA, 100 ng ml^{-1}) (B), and FA plus tunicamycin (TUN, 50 ng ml^{-1}). Transwells were counterstained with DAPI (C), and quantified (D). Different letters denote differences among groups (a ≠ b ≠ c, denote $P < 0.05$).

then trypsin harvested and seeded at 50 000 cells per insert in 250 μl of serum free medium. Thereafter, HTR8/SVneo cell's growth medium supplemented with folic acid (100 ng ml^{-1}, 0.1% v/v, 750 μl) or folic acid plus tunicamycin (50 ng ml^{-1}, 0.1% v/v) was added to the lower insert chamber. After 18 h incubation, non-invading cells were removed using a cotton swab from the upper side of the membrane. The invaded cells that penetrated the membrane were fixed with 10% neutral-buffered formalin for 30 min at RT, then stained with DAPI for quantification. All treatments were run in triplicate.

Statistical analysis

All data are presented as mean ± SEM. Appropriate transformations were applied, as needed, to account for normality of data. To evaluate significance, differences among treatment groups were analyzed using ANOVA with Tukey *post hoc* tests for transwell invasion, and general mixed model with Dunnett *post hoc* tests for extracellular matrix, microfluidic chip invasion, and cytotoxicity assays. Statistical software used was PASW Statistics for Windows release 18.0.1. Differences were considered significant at $P < 0.05$.

Results and discussion

Optimization of 3D microfluidic chip culture conditions

The ECM is a non-cellular component of tissues that supports cell adhesion. ECMs used in this study (Matrigel, gelatin and fibronectin) have all been previously used to coat organ-on-a-chip microfluidic device models of intestine,[35] skeletal muscle,[36] and liver.[37] Although the use of ECM matrices are not often reported in 3D microfluidic systems,[20] cells often show different growth and attachment responses to different ECMs.[38] Therefore, we tested three matrices and compared cell adhesion in uncoated (control) dishes and all three ECM-coated (gelatin, Matrigel and fibronectin) dishes. While all ECMs tested were able to support HTR8/SVneo cells' attachment at all time points (2, 3, and 4 h; Fig. 2A, Fig. S1A†), fibronectin had the highest cell attachment in both HTR8/SVneo and HUVEC cells, followed by Matrigel and gelatin (Fig. 2A and B and S1A and B†). This effect was more pronounced in HTR8/SVneo cells (Fig. 2A). Localization of the HTR8/SVneo-mCherry and HUVEC cells within the 3D microfluidic chip and Z-stack plot are shown in Fig. S2.† When testing the three matrices in the 3D microfluidic chip, fibronectin also displayed the best ability to support adhesion for both cell types (Fig. 2C). The suitability of fibronectin may be because it is secreted from placental cells[39] and/or because the basement membrane and stroma of the placenta villi are enriched for fibronectin, compared to gelatin and Matrigel.[40–43] Fibronectin enables growth of both endothelial and trophoblast cells by binding to integrins and other ECM proteins, playing a critical role in cell adhesion.[44–46] Consistent with our findings, fibronectin has also been used in other human placenta microfluidic models focused on drug transport and cell fusion.[20,21,47] Although Matrigel has been used in some 3D placenta models,[22,23] it may not be ideal for studying EVT migration as it is less stiff than the decidua basalis.[48] Additionally, Matrigel is a complex mixture of known growth factors that can affect trophoblast invasion[49] and other proteins of unknown functions in culture.[50] Batch-to-batch variation in protein content is another concern of using Matrigel.[48] On the other hand, gelatin, a natural biopolymer capable of modulating cell adhesion, was also tested in a 3D trophoblast invasion

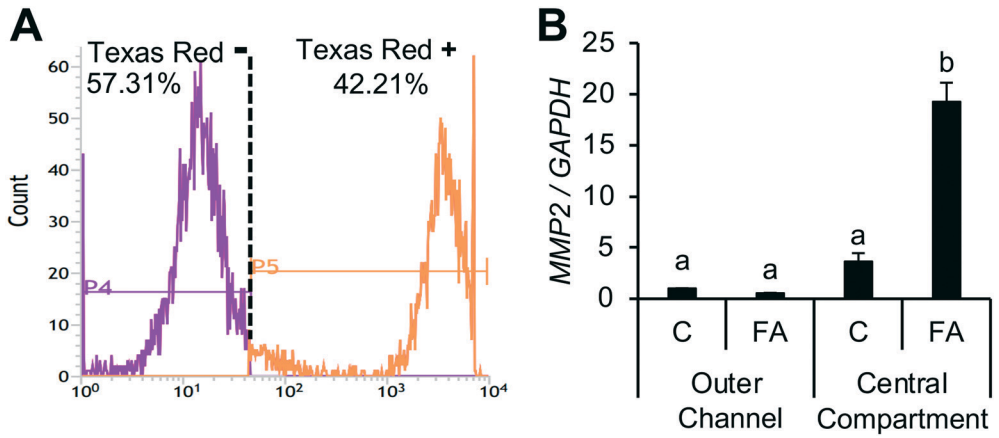

Fig. 8 Flow cytometry and gene expression after invasion assay in the 3D microfluidic chip. After 3 days of culture (culture conditions: fibronectin, 30 million cells per ml, and 0.01 μl min^{-1} flow), cells in central compartment and outer channels were trypsin-digested and harvested for cell sorting (see Methods for details). (A) Representative flow cytometry result for Texas Red^{+} (right, mCherry tagged HTR8/SVneo cells) and Texas Red^{-} (left, HUVECs cells) of cells in the central compartment. (B) Matrix metalloproteinase-2 (MMP2) mRNA expression in sorted Texas Red^{+} cells from the central compartment and outer channels in control (C) and folic acid (FA) groups. Different letters denote differences among groups (a ≠ b denote $P < 0.05$).

model.[13] Although the stiffness of the gelatin can be adjusted in the range of the native tissue, the cross-linking density of gelatin has been reported to affect the formation of a functional endothelial cell monolayer.[13,51]

Since cell seeding density *in vitro* can often change cells' adhesion and proliferation, determining the cell density is key to establish a proper endothelial layer. We tested 3 different cell seeding densities (10, 20, and 30 million cells per ml) in fibronectin pre-coated 3D microfluidic chips (Fig. S3†). HTR8/SVneo cells and HUVECs seeded at the highest density (30 million cells per ml) formed a confluent intact cell layer after they attached (Fig. S4†). In this work, the highest HUVEC cell density (30 million cells per ml) provided the best cell surface area coverage. Seeding an insufficient cell population will result in a non-intact endothelial layer or in sparsely covered regions on the matrix gel surface.[13,51] In our experience, ensuring that an intact HTR8/SVneo cell layer covers the entire barrier surfaces in the outer channels is essential to minimize variability among replicates. Previously reported human placenta microfluidic models have used lower cell seeding densities (1–8 million cells per ml),[20–23,47] but to our knowledge, cell density testing has not been reported for any of these models. Structure and channel volume parameters vary across microfluidic models, resulting in differences in cell seeding densities. Therefore, each 3D microfluidic chip type should be carefully optimized for each cell type used and application tested.

An advantage of this 3D model system is that it allows for continuous medium perfusion providing constant replenishment of nutrient supplementation within the microfluidic chip. Media flow also provides fluidic shear stress that occurs in the placental microenvironment. The flow speeds tested in the 3D microfluidic chip (0.01, 0.05 and 0.1 μl min^{-1}) had liquid shear stresses of 0.0046, 0.0228, and 0.0457 N m^{-2}, respectively. All resulted in similar cell morphology and confluency after a 24 h culture period (Fig. S4†). Flow speeds used in this study were slower than those previously reported in other placenta microfluidic chips (30–100 μl h^{-1}).[20–23,52] To note is that the calculated shear stresses do not account for changes in channel directionality, resistance from the ECM coating, and cell coverage of the channels. Given the importance of shear stress on the cell docking process,[53] slower flow speeds were used to prevent invading cells from being flushed through the outer compartments by higher flow speed, particularly during the early stages of invasion. However, changes in shear stress can alter cell fate and transcriptomics,[54] and should thus be further explored and standardized for each cell type. To limit the potential effect of a strong shear stress, the lowest flow speed (0.01 μl min^{-1}) along with the highest cell density were chosen for the permeability assay.

Characterization of the 3D microfluidic chip endothelial–trophoblast placental barrier

The integrity of the endothelial cell layer ensures proper barrier permeability for the trafficking of macromolecules.[55] Since fluid shear stress can alter endothelial permeability,[56,57] using the standardized conditions (fibronectin, 30 million cells per ml, and 0.01 μl min^{-1} flow speed), we evaluated the endothelial–trophoblast barrier using a permeability assay. We used a fluorescently labelled dextran (FITC-dextran) to create a concentration gradient of diffusible molecules between the outer channels and the central compartment. Without cells seeded, our model allowed the FITC-dextran to diffuse through the barrier, reaching the center of the central compartment within 2 min (Fig. 3A–F). We evaluated FITC-dextran diffusion (Fig. 3) and determined that the endothelial cell layer (central compartment) acted as placental barrier by blocking

diffusion for ~48 h (Fig. 3G–I). The cell layers on the pillar barrier restricted the diffusion of FITC-dextran into the central compartment and resulted in a gradual build-up gradient reaching the center of the central compartment by 72 h (Fig. 3G–I). To test the effect of flow speed on the cell barrier permeability, the FITC-dextran diffusion was tested at a faster flow speed (10 μl min^{-1}), which resulted in the FITC-dextran reaching the center of the central compartment by 6 h, compared with 48 h at 0.1 μl min^{-1} (Fig. 3J–M). This supports previous findings where shear stress increases endothelial cell's permeability.[58] Flow-driven changes in permeability support the successful establishment of an endothelial barrier in this model.

Cell invasion in the 3D microfluidic chip upon treatment

We first confirmed HTR8/SVneo cells' invasiveness ability using a matrix degradation assay (Fig. S5†). Folic acid, commonly supplemented during pregnancy for the prevention of neural tube defects, has been shown to stimulate EVT cell invasion by modulating MMP-2 expression.[59,60] Thus, to validate the current 3D invasion model we used folic acid as a positive control. After 5 days of exposure in HTR8/SVneo, folic acid was not cytotoxic at any dose tested while tunicamycin was cytotoxic starting at 100 ng ml^{-1} (Fig. S6†). HTR8/SVneo-mCherry invasiveness was tested in co-culture with HUVEC cells in the 3D microfluidic chip and cultured for 3 days with medium flow (0.01 μl min^{-1}) (Fig. 4). Localization of HTR8/SVneo-mCherry and HUVEC cells in the 3D microfluidic chip after immunostaining with endothelial cell marker protein, vWF is shown in Fig. 5. HTR8/SVneo cells begun to spontaneously invade after 12 h (data not shown) and can be clearly visualized in the central compartment after 24 h (Fig. 6). We demonstrated that within the 3D microfluidic model HTR8/SVneo cells displayed invasion upon folic acid exposure (Fig. 6 and S8†). Folic acid's enhancement of trophoblast cell invasion was similar to that of previous studies[59,60] and to that of our internal validation in the transwell system (Fig. 7). We were also able to counteract folic acid-induced invasion with tunicamycin, which is known to inhibit human trophoblast cell invasion by inducing endoplasmic reticulum stress.[31]

To test whether the presence of the endothelial cells would affect HTR8/SVneo cells' invasiveness, we also exposed HTR8/SVneo cells to folic acid and/or tunicamycin in the absence of HUVEC cells. Folic acid enhanced HTR8/SVneo cell invasiveness in the absence of HUVEC cells, although this effect was more marked than when HUVEC cells were present (Fig. 6). While the absence of HUVEC cells may result in a lack of cytokines and growth factors that enhance trophoblast invasion,[49,61] the enhanced invasion of HTR8/SVneo in the absence of HUVECs observed here likely relates to faster diffusion of the chemoattractant and nutrients (serum) from central compartment to the outer channels, and to the lack of physical barrier created by the presence of HUVEC cells. In the 3D microfluidic chip, it is possible to visualize the cell-to-cell interactions between HTR8/SVneo and HUVEC cells. Immunostaining of the transmigration protein ICAM-1, which is enriched in endothelial cells upon interaction with invasive cells,[62,63] was enhanced in HUVEC cells in close contact with invading HTR8/SVneo cells (Fig. S7†).

Compared to previous models that only allow for a static endpoint (*i.e.* transwell), this new platform, in combination with fluorescent cell tagging, allows tracking of EVT invasion in real-time and can be run over the course of several days. Coupled with fluorescent cell tagging, we have been able to sort invasive cells using flow cytometry, a noted future direction in earlier studies.[23] After cell sorting, we observed that MMP-2 mRNA expression, a critical factor in controlling trophoblast invasion at the maternal–fetal interface,[27,64,65] was upregulated in HTR8/SVneo cells that invaded into central compartment compared to those that remained in the outer channels (Fig. 8 and S9†). The ability to harvest invasive cells provides an outstanding tool to investigate cellular signatures during trophoblast cell invasion.

Despite the advantages of this model, there are still several limitations. One of them is the low throughput of the system, as each chip needs to be connected to a pump that can run a limited number of media channels. Preconditioning of the microfluidic chip is also very labor intensive and requires skilled management. Another limitation of the model relates to the design of the chip. While the circular barrier design was ideal during the conceptual phase of the project, future studies should allow for a scaling-up of the lateral compartment so that the number of invasive cells in the initial seeding is not as limited. This allows for a greater cellular output that can be further used for flow cytometry and gene expression analysis. In contrast to other studies that have used primary trophoblasts,[23] in this study, similar to others,[20,22,66] we used an EVT cell line. The use of a well characterized cellular model of placental invasion[14,27,28] allowed for a thorough standardization of the model. Although challenging, future studies should focus on incorporating primary EVTs into 3D microfluidic models.

Conclusion

In this study, we have developed a novel 3D microfluidic platform that recreates the placental invasion microenvironment. Using a commercially available 3D microfluidic chip, this platform reproduces key elements of the human placental barrier, including an extracellular matrix (ECM), a two-cell interface of human endothelial (HUVEC) and extravillous trophoblast (HTR8/SVneo) cells, and a dynamic flow exchange that allows for the delivery of a chemical gradient. This new platform resembling the placental microenvironment allows real-time monitoring, harvesting of invasive cells through flow cytometry, and evaluation of heterocellular cell-to-cell interactions. We have

tested invasiveness in this platform using two known chemoattractants and validated it using the well-established transwell invasion assay. Altogether, this model can be used in toxicological testing, with invasion as the target endpoint, in a complex organ such as the placenta.

Conflicts of interest

The authors declare no conflict of interest.

Acknowledgements

This work was supported by an Alternative Research Grant of the Society of Toxicology and the National Institute of Environmental Health Sciences of the National Institute of Health under award number R01ES027863 to AV-L. Funding for J. G. was supported by the Eunice Kennedy Shriver National Institute of Child Health & Human Development of the National Institutes of Health (NICHD) under award number T32HD087166. The content is solely the responsibility of the authors and does not necessarily represent the official views of the National Institutes of Health. We thank Dr. Carlos Murga-Zamalloa for gifting the lentivirus packaging system.

References

1 E. Menkhorst, A. Winship, M. Van Sinderen and E. Dimitriadis, *Reprod., Fertil. Dev.*, 2016, **28**, 406–415.
2 L. Lunghi, M. E. Ferretti, S. Medici, C. Biondi and F. Vesce, *Reprod. Biol. Endocrinol.*, 2007, **5**, 6.
3 K. H. Lim, Y. Zhou, M. Janatpour, M. McMaster, K. Bass, S. H. Chun and S. J. Fisher, *Am. J. Pathol.*, 1997, **151**, 1809–1818.
4 G. Barrientos, M. Pussetto, M. Rose, A. C. Staff, S. M. Blois and J. E. Toblli, *Mol. Hum. Reprod.*, 2017, **23**, 509–519.
5 N. J. Sebire, H. Fox, M. Backos, R. Rai, C. Paterson and L. Regan, *Hum. Reprod.*, 2002, **17**, 1067–1071.
6 G. J. Burton, E. Jauniaux and D. S. Charnock-Jones, *Int. J. Dev. Biol.*, 2010, **54**, 303–312.
7 G. J. Burton, A. L. Watson, J. Hempstock, J. N. Skepper and E. Jauniaux, *J. Clin. Endocrinol. Metab.*, 2002, **87**, 2954–2959.
8 L. K. Harris, S. D. Smith, R. J. Keogh, R. L. Jones, P. N. Baker, M. Knofler, J. E. Cartwright, G. S. Whitley and J. D. Aplin, *Am. J. Pathol.*, 2010, **177**, 2103–2115.
9 J. Pollheimer, S. Vondra, J. Baltayeva, A. G. Beristain and M. Knofler, *Front. Immunol.*, 2018, **9**, 2597.
10 S. Xiong, A. M. Sharkey, P. R. Kennedy, L. Gardner, L. E. Farrell, O. Chazara, J. Bauer, S. E. Hiby, F. Colucci and A. Moffett, *J. Clin. Invest.*, 2013, **123**, 4264–4272.
11 A. Albini, Y. Iwamoto, H. K. Kleinman, G. R. Martin, S. A. Aaronson, J. M. Kozlowski and R. N. McEwan, *Cancer Res.*, 1987, **47**, 3239–3245.
12 M. E. Katt, A. L. Placone, A. D. Wong, Z. S. Xu and P. C. Searson, *Front. Bioeng. Biotechnol.*, 2016, **4**, 12.
13 S. G. Zambuto, K. B. H. Clancy and B. A. C. Harley, *Interface Focus*, 2019, **9**, 20190016.
14 M. K. Wong, M. Wahed, S. A. Shawky, A. Dvorkin-Gheva and S. Raha, *Sci. Rep.*, 2019, **9**, 12607.
15 N. Kramer, A. Walzl, C. Unger, M. Rosner, G. Krupitza, M. Hengstschlager and H. Dolznig, *Mutat. Res.*, 2013, **752**, 10–24.
16 R. Mittal, F. W. Woo, C. S. Castro, M. A. Cohen, J. Karanxha, J. Mittal, T. Chhibber and V. M. Jhaveri, *J. Cell. Physiol.*, 2019, **234**, 8352–8380.
17 R. L. Pemathilaka, D. E. Reynolds and N. N. Hashemi, *Interface Focus*, 2019, **9**, 20190031.
18 K. H. Benam, R. Novak, J. Nawroth, M. Hirano-Kobayashi, T. C. Ferrante, Y. Choe, R. Prantil-Baun, J. C. Weaver, A. Bahinski, K. K. Parker and D. E. Ingber, *Cell Syst.*, 2016, **3**, 456–466.
19 J. Lee, R. Romero, Y. M. Han, H. C. Kim, C. J. Kim, J. S. Hong and D. Huh, *J. Matern.-Fetal Neonat. Med.*, 2016, **29**, 1046–1054.
20 C. Blundell, E. R. Tess, A. S. Schanzer, C. Coutifaris, E. J. Su, S. Parry and D. Huh, *Lab Chip*, 2016, **16**, 3065–3073.
21 C. Blundell, Y. S. Yi, L. Ma, E. R. Tess, M. J. Farrell, A. Georgescu, L. M. Aleksunes and D. Huh, *Adv. Healthcare Mater.*, 2018, **7**(2), DOI: 10.1002/adhm.201700786.
22 F. C. Yin, Y. J. Zhu, M. Zhang, H. Yu, W. W. Chen and J. H. Qin, *Toxicol. In Vitro*, 2019, **54**, 105–113.
23 Y. Abbas, C. M. Oefner, W. J. Polacheck, L. Gardner, L. Farrell, A. Sharkey, R. Kamm, A. Moffett and M. L. Oyen, *J. R. Soc., Interface*, 2017, **14**(130), 20170131.
24 C. H. Graham, T. S. Hawley, R. G. Hawley, J. R. MacDougall, R. S. Kerbel, N. Khoo and P. K. Lala, *Exp. Cell Res.*, 1993, **206**, 204–211.
25 H. Msheik, J. Azar, M. El Sabeh, W. Abou-Kheir and G. Daoud, *Placenta*, 2020, **90**, 90–97.
26 W. Abou-Kheir, J. Barrak, O. Hadadeh and G. Daoud, *Placenta*, 2017, **50**, 1–7.
27 Y. Li, C. Klausen, H. Zhu and P. C. Leung, *J. Clin. Endocrinol. Metab.*, 2015, **100**, E1415–E1427.
28 H. J. Zhao, C. Klausen, Y. Li, H. Zhu, Y. L. Wang and P. C. K. Leung, *Cell Death Dis.*, 2018, **9**, 174.
29 E. Frohlich, G. Bonstingl, A. Hofler, C. Meindl, G. Leitinger, T. R. Pieber and E. Roblegg, *Toxicol. In Vitro*, 2013, **27**, 409–417.
30 P. J. Williams, J. N. Bulmer, B. A. Innes and F. Broughton Pipkin, *Biol. Reprod.*, 2011, **84**, 1148–1153.
31 C. L. Lee, J. H. W. Veerbeek, T. K. Rana, B. B. van Rijn, G. J. Burton and H. W. Yung, *Am. J. Pathol.*, 2019, **189**, 467–478.
32 Y. Pu, S. Pearl, J. Gingrich, J. Jing, D. Martin, C. A. Murga-Zamalloa and A. Veiga-Lopez, *Arch. Toxicol.*, 2019, **93**, 1665–1677.
33 K. H. Martin, K. E. Hayes, E. L. Walk, A. G. Ammer, S. M. Markwell and S. A. Weed, *J. Visualized Exp.*, 2012, e4119, DOI: 10.3791/4119.
34 Y. Pu, J. D. Gingrich, J. P. Steibel and A. Veiga-Lopez, *Endocrinology*, 2017, **158**(11), 3844–3858.
35 M. Chi, B. Yi, S. Oh, D. J. Park, J. H. Sung and S. Park, *Biomed. Microdevices*, 2015, **17**, 9966.

36 Y. Wei, F. Chen, T. Zhang, D. Chen, X. Jia, J. Wang, W. Guo and J. Chen, *Sci. Rep.*, 2015, **5**, 14049.
37 L. Prodanov, R. Jindal, S. S. Bale, M. Hegde, W. J. McCarty, I. Golberg, A. Bhushan, M. L. Yarmush and O. B. Usta, *Biotechnol. Bioeng.*, 2016, **113**, 241–246.
38 S. Schlie-Wolter, A. Ngezahayo and B. N. Chichkov, *Exp. Cell Res.*, 2013, **319**, 1553–1561.
39 A. K. Nanaev, A. P. Milovanov and S. P. Domogatsky, *Histochemistry*, 1993, **100**, 341–346.
40 B. A. Bray, *J. Clin. Invest.*, 1978, **62**, 745–752.
41 U. Earl, C. Estlin and J. N. Bulmer, *Placenta*, 1990, **11**, 223–231.
42 M. Isemura, Y. Yamaguchi, H. Munakata, K. Kurosawa, T. Furuyama, K. Yoshinaga, T. Masuda, H. Nagai, M. Motomiya and Z. Yosizawa, *Tohoku J. Exp. Med.*, 1985, **145**, 373–379.
43 T. Yamada, M. Isemura, Y. Yamaguchi, H. Munakata, N. Hayashi and M. Kyogoku, *Histochemistry*, 1987, **86**, 579–584.
44 E. W. Young, A. R. Wheeler and C. A. Simmons, *Lab Chip*, 2007, **7**, 1759–1766.
45 R. A. Clark, P. DellaPelle, E. Manseau, J. M. Lanigan, H. F. Dvorak and R. B. Colvin, *J. Invest. Dermatol.*, 1982, **79**, 269–276.
46 B. X. Zeng, H. Fujiwara, Y. Sato, Y. Nishioka, S. Yamada, S. Yoshioka, M. Ueda, T. Higuchi and S. Fujii, *J. Reprod. Immunol.*, 2007, **73**, 1–10.
47 J. S. Lee, R. Romero, Y. M. Han, H. C. Kim, C. J. Kim, J. S. Hong and D. Huh, *J. Matern.-Fetal Neonat. Med.*, 2016, **29**, 1046–1054.
48 Y. Abbas, A. Carnicer-Lombarte, L. Gardner, J. Thomas, J. J. Brosens, A. Moffett, A. M. Sharkey, K. Franze, G. J. Burton and M. L. Oyen, *Hum. Reprod.*, 2019, **34**, 1999–2008.
49 M. Knofler, *Int. J. Dev. Biol.*, 2010, **54**, 269–280.
50 C. S. Hughes, L. M. Postovit and G. A. Lajoie, *Proteomics*, 2010, **10**, 1886–1890.
51 C. D. Cook, A. S. Hill, M. Guo, L. Stockdale, J. P. Papps, K. B. Isaacson, D. A. Lauffenburger and L. G. Griffith, *Integr. Biol.*, 2017, **9**, 271–289.
52 J. S. Lee, R. Romero, Y. M. Han, H. C. Kim, C. J. Kim, J. S. Hong and D. Huh, *J. Matern.-Fetal Neonat. Med.*, 2016, **29**(7), 1046–1054.
53 M. Cioffi, M. Moretti, A. Manbachi, B. G. Chung, A. Khademhosseini and G. Dubini, *Biomed. Microdevices*, 2010, **12**, 619–626.
54 C. M. Metallo, M. A. Vodyanik, J. J. de Pablo, I. I. Slukvin and S. P. Palecek, *Biotechnol. Bioeng.*, 2008, **100**, 830–837.
55 D. Mehta, K. Ravindran and W. M. Kuebler, *Am. J. Physiol.*, 2014, **307**, L924–L935.
56 J. A. LaMack, H. A. Himburg, X. M. Li and M. H. Friedman, *Ann. Biomed. Eng.*, 2005, **33**, 457–464.
57 J. Zhou, Y. S. Li and S. Chien, *Arterioscler., Thromb., Vasc. Biol.*, 2014, **34**, 2191–2198.
58 H. S. Bevan, S. C. Slater, H. Clarke, P. A. Cahill, P. W. Mathieson, G. I. Welsh and S. C. Satchell, *Am. J. Physiol.*, 2011, **301**, F733–F742.
59 L. Zhou, A. Zhang, K. Wang, Q. Zhou and T. Duan, *Int. J. Clin. Exp. Pathol.*, 2015, **8**, 3008–3014.
60 T. Ahmed, I. Fellus, J. Gaudet, A. J. MacFarlane, B. Fontaine-Bisson and S. A. Bainbridge, *Placenta*, 2016, **37**, 7–15.
61 G. Weiss, B. Huppertz, M. Siwetz, I. Lang and G. Moser, *Placenta*, 2016, **38**, 49–56.
62 C. V. Carman and T. A. Springer, *Curr. Opin. Cell Biol.*, 2008, **20**, 533–540.
63 P. Alcaide, S. Auerbach and F. W. Luscinskas, *Microcirculation*, 2009, **16**, 43–57.
64 A. Onogi, K. Naruse, T. Sado, T. Tsunemi, H. Shigetomi, T. Noguchi, Y. Yamada, M. Akasaki, H. Oi and H. Kobayashi, *Placenta*, 2011, **32**, 665–670.
65 Y. Zhang, F. Jin, X. C. Li, F. J. Shen, X. L. Ma, F. Wu, S. M. Zhang, W. H. Zeng, X. R. Liu, J. X. Fan, Y. Lin and F. J. Tian, *Mol. Ther.*, 2017, **25**, 2394–2403.
66 J. S. Lee, R. Romero, Y. M. Han, H. C. Kim, C. J. Kim, J. S. Hong and D. Huh, *J. Matern.-Fetal Neonat. Med.*, 2016, **29**, 1046–1054.

